

Review

Supramolecular Approaches to Nanoscale Morphological Control in Organic Solar Cells

Alexander M. Haruk ^{1,2} and Jeffrey M. Mativetsky ^{1,*}

¹ Department of Physics, Applied Physics and Astronomy, Binghamton University, Binghamton, NY 13902, USA

² Department of Chemistry, Binghamton University, Binghamton, NY 13902, USA;
E-Mail: aharuk1@binghamton.edu

* Author to whom correspondence should be addressed; E-Mail: jmativet@binghamton.edu;
Tel.: +1-607-777-4352; Fax: +1-607-777-2546.

Academic Editor: John George Hardy

Received: 23 May 2015 / Accepted: 8 June 2015 / Published: 11 June 2015

Abstract: Having recently surpassed 10% efficiency, solar cells based on organic molecules are poised to become a viable low-cost clean energy source with the added advantages of mechanical flexibility and light weight. The best-performing organic solar cells rely on a nanostructured active layer morphology consisting of a complex organization of electron donating and electron accepting molecules. Although much progress has been made in designing new donor and acceptor molecules, rational control over active layer morphology remains a central challenge. Long-term device stability is another important consideration that needs to be addressed. This review highlights supramolecular strategies for generating highly stable nanostructured organic photovoltaic active materials by design.

Keywords: solar cells; organic semiconductors; morphology; supramolecular interactions; self-assembly; nanowires; device stability

1. Introduction

Solar cells based on organic molecules offer a potentially low-cost, mechanically-flexible, and lightweight platform for the clean conversion of sunlight to electricity [1–5]. From a research and development standpoint, organic solar cells, or organic photovoltaics (OPV), offer several advantages

that make them promising alternatives to their inorganic counterparts. The high extinction coefficient of organic semiconductors allows for a reduction in the amount of material needed to harvest incoming photons [1,6]. Chemical synthesis provides fine-tuning of the chemical structure, and in turn, the optical and electrical properties of the active materials [1,4,7,8]. These materials are also easily processed from solution near room temperature and have great potential for low-cost industrial scale manufacturing by roll-to-roll processing and spray-coating [2,9,10].

Over the past decade, the efficiency of lab-scale organic solar cells has more than doubled, to beyond 10% [11–13]. The highest performance organic solar cells rely on a bicomponent nanostructured active layer morphology. Despite the key role of this nanostructuring in dictating device performance [2,6,14–21], predictive control over active layer structure remains a pivotal challenge. Moreover, because nanostructuring is often achieved through the formation of metastable phases, active layer stability, especially at elevated temperatures, is also of concern [2,6,16,22].

Supramolecular, *i.e.*, non-covalent, interactions offer a means of manipulating the assembly of organic systems [23–28]. Through judicious molecular design, specific molecular assembly motifs can be “programmed”. Supramolecular approaches have only recently begun to be applied to OPV systems, to promising effect. In this review, we examine supramolecular strategies for tailoring and stabilizing the nanoscale morphology of organic solar cell active layers. After introducing the basic operating principles of organic solar cells, we will highlight OPV systems that are designed to harness aromatic stacking, hydrogen bonding, and shape complementarity in order to improve the nanomorphology, performance, and stability of OPV active layers.

2. Working Principles of Organic Solar Cells

Organic solar cell active layers consist of two organic semiconductors, one serving as an electron donor and the other as an electron acceptor. Absorption of a photon leads to the generation of an exciton, a short-lived bound electron-hole pair. Due to the high binding energy of excitons in organic semiconductors [2,16], the exciton cannot dissociate unless it diffuses to a donor–acceptor interface, where it is energetically favorable to separate into free charges (see Figure 1A,B) [2]. For the charges to be collected, the electron must travel through the acceptor to the cathode while the hole must travel through the donor to the anode [2,6,16,29,30].

For efficient organic solar cell operation, two competing length scale requirements must be satisfied: (1) the light absorbing layer must be hundreds of nanometers thick for efficient light absorption; and (2) the light-induced generation of excitons must occur within about 10 nm of a donor–acceptor interface for separation into free charge carriers [3,7,14,22], otherwise the light-generated excitation will be lost to recombination. The bulk-heterojunction concept [3,6,15,22,31] cleverly satisfies both requirements through the use of nanoscale interpenetrating donor and acceptor domains, as illustrated in Figure 1C. In bulk-heterojunction solar cells, the light-capturing film is sufficiently thick to absorb most incoming light, while the high density of donor–acceptor interfaces provides efficient charge generation. In practice, in addition to pure domains, finely mixed donor–acceptor regions are also commonly present on account of donor–acceptor miscibility [22,32–35]. Continuous charge transport pathways are required for holes to percolate through the donor to the anode, and electrons to percolate through the acceptor to the cathode. Molecular orientation, molecular packing structure, and the degree of

intermolecular order also significantly impact charge transport efficiency [36–45]. Domain dimensions, continuity, and internal structure are therefore key features that govern OPV performance.

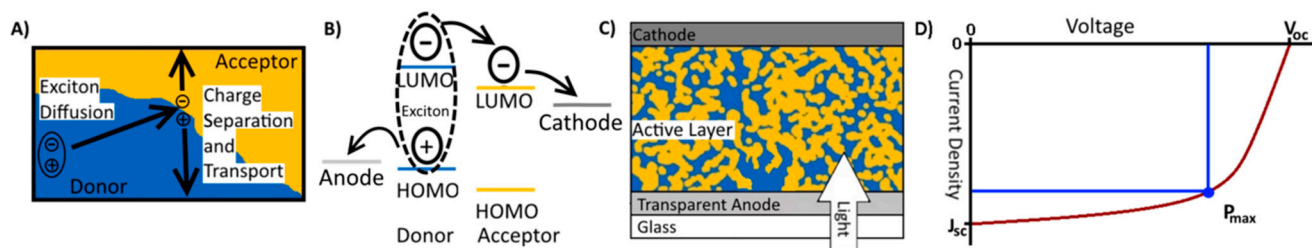


Figure 1. (A) Schematic of the main processes that take place in an organic solar cell; (B) Corresponding energy level diagram; (C) Bulk heterojunction solar cell structure; (D) Typical electrical characteristics of an organic solar cell with the J – V curve in red and the current density and voltage at P_{\max} shown in blue.

Solar cell performance is measured by recording current density J , *i.e.*, current per device area, as a function of voltage V (see Figure 1D). The short-circuit current density J_{sc} is the current density when there is no voltage difference between the anode and cathode. The J_{sc} is influenced by the amount of light that is absorbed, the exciton separation efficiency, and the ability of the free charges to reach the electrodes [30]. The open circuit voltage V_{oc} is the voltage across the device when there is no net flow of current, and is predominantly dependent on the difference between the highest occupied molecular orbital (HOMO) of the donor and the lowest unoccupied molecular orbital (LUMO) of the acceptor, while also being influenced by the electrode work function [1,46–49]. The fill factor (FF), associated with the “squareness” of the J – V curve, is defined as the ratio of the maximum power density of the cell P_{\max} and the theoretical maximum power density based on J_{sc} and V_{oc} :

$$FF = \frac{P_{\max}}{J_{\text{sc}} V_{\text{oc}}} \quad (1)$$

Power conversion efficiency (PCE) is the percentage associated with the ratio of the maximum power density and the power density of the incident light:

$$PCE = \frac{P_{\max}}{P_{\text{in}}} \times 100\% \quad (2)$$

The series resistance R_s is the internal resistance of the device, and the shunt resistance R_{sh} is a measure of the resistance to current leakage in the device [7].

Nanostructured bulk heterojunction active layers are typically achieved by casting a thin film from a donor–acceptor co-solution, and using thermal annealing, additives, or other means to promote phase separation [2,22,50,51]. The resulting morphology is governed by a complex interplay between film formation kinetics, component miscibility, and crystallization, making the associated solar cell performance highly sensitive to the precise processing conditions [16,22,46,52]. The design of donor–acceptor systems with specified supramolecular interactions provides opportunities to tailor organic solar cell active layer structure, which plays such a critical role in device operation.

3. Aromatic Stacking

Aromatic stacking results from the interactions between π -orbitals of separate π -systems. For organic semiconductors, with their large, often planar, conjugated π -systems, this can result in a face–face interaction between the molecules. In this arrangement, charge transport is favored along the stacking direction [38,39,53–56]. This section will discuss how aromatic stacking has been harnessed to form nanowires, manipulate active layer domain size, and mediate donor–acceptor interactions.

3.1. Self-Assembled Nanowires

Nanowires are promising for achieving high performance in organic solar cells as they present both a large surface-to-volume ratio, essential for charge separation, and a continuous conduit for charge collection. The most common methods for generating organic semiconductor nanowires involve the addition of a poor solvent, or gradual cooling of a warm saturated solution, in order to slowly induce aggregation and precipitation of the organic semiconductor [30,57–64]. A widely-studied class of polymer donor, poly(3-alkylthiophene) (P3AT), forms nanowires through face-to-face stacking of the polymer backbone, with the stacking direction being parallel to the long axis of the wire (see Figure 2) [30,58,65]. This long-range face-to-face packing leads to efficient hole transport along the wire axis [58,59,65].

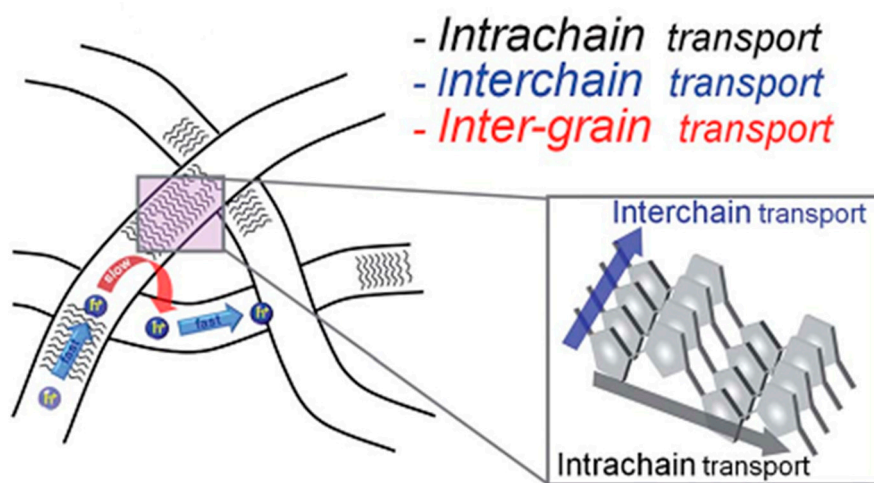


Figure 2. Schematic of the face-face stacking of polymer chains in P3AT nanowires. Reproduced from [58] with permission from The Royal Society of Chemistry.

As shown in Figure 3, in OPV active layers, P3AT nanowires form a network of continuous pathways for charge to travel through [30,57–60]. For a 100 nm thick active layer, poly-3-hexylthiophene (P3HT):phenyl-C₆₁-butyric acid methyl ester (PCBM) devices that incorporated P3HT nanowires outperformed conventional bulk heterojunctions. The improved performance in the nanowire-based solar cells was proposed to stem from the 15-fold higher hole mobility in the active layer [60], which resulted in a near unity electron/hole mobility balance. A mismatch between electron and hole mobility can hinder device performance though a build-up of space charge [66,67].

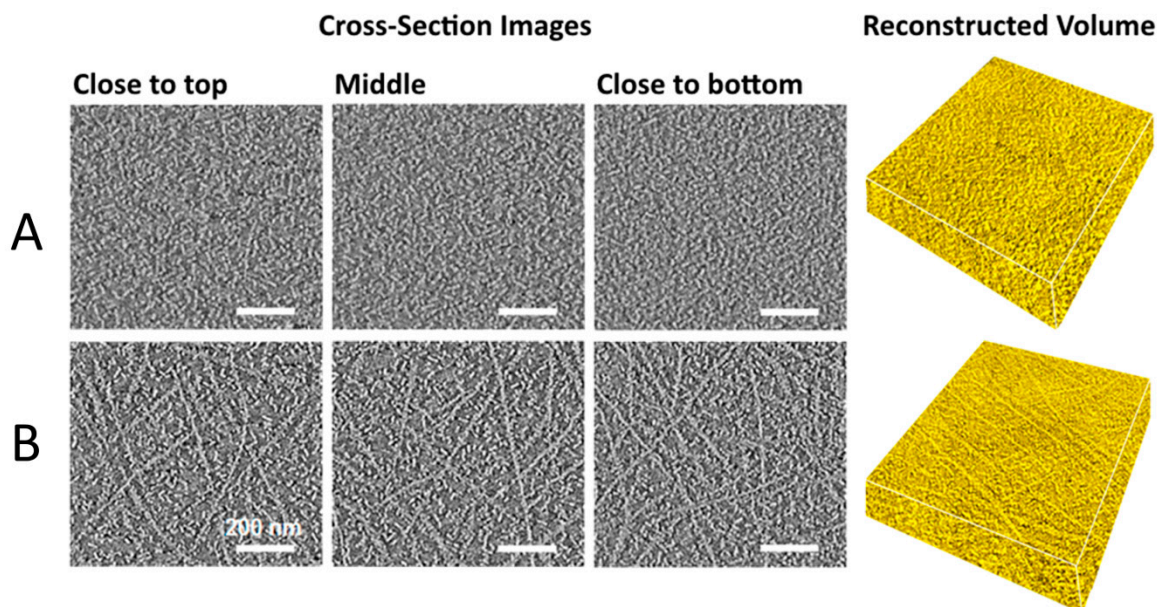


Figure 3. Cross-section images obtained by electron tomography from the top to bottom along the plane of the active layer for (A) a conventional bulk heterojunction and (B) a nanowire-based heterojunction, with reconstructed $900 \times 900 \times 200$ nm volumes. Adapted from [60] with permission from the American Chemical Society. Scale bar: 200 nm.

As the active layer thickness was increased, conventional devices saw a worsening of the mobility imbalance and an increase in R_s , while the nanowire devices maintained well-balanced electron and hole mobilities, and a low R_s [60]. In other words, the nanowire-based active layers better maintained percolation pathways for charge collection, even in relatively thick films. The J_{sc} of nanowire devices increased with thickness, up to 300 nm, while the V_{oc} and FF remained constant. The improved J_{sc} was attributed to the increased light absorption of the thicker active layer. The top-performing nanowire device had a PCE of 4.21%, 46% higher than the optimized conventional device [60]. This study demonstrates the potential merits of nanowire based solar cells: better charge percolation enables the use of thicker active layers, which in turn improves light absorption by the device. Active layers that are hundreds of nanometers thick are also more amenable to large-scale manufacturing than thinner layers [9,58].

Another important property of a nanowire is the aspect ratio, *i.e.*, the ratio of length to diameter. Self-assembled nanowires formed from poly(3-butylthiophene)-*b*-poly(3-octylthiophene) diblock copolymers maintained a width of 13–16 nm, but had a composition dependent aspect ratio (ranging from 48 to 263), depending on the relative amount of each block. Active layers incorporating wires with the largest aspect ratio had the highest J_{sc} , which was attributed to these wires providing superior charge transport and collection over longer length scales [59].

Nanowires have also been employed to improve the performance of lateral organic solar cells (LOSC), in which the cathode and anode are laterally spaced, with the active layer in between. This unconventional architecture has the advantage that it does not require a transparent electrode; however, efficiencies thus far have been limited, largely owing to the relatively long distances over which charges must be transported to reach the electrodes, typically hundreds of nanometers to tens of micrometers [68–70]. Due to the favorable charge transport properties and durability of P3HT

nanowires, it was possible to make a flexible device with a PCE of 2% under low light intensity (0.1 Sun), that was able to retain 95% of its efficiency after extended stress testing [71]. Bimolecular recombination of charge carriers was a dominant mechanism for performance loss, likely owing to the long channel length over which electrons and holes must be transported for collection at the cathode and anode. This was particularly apparent under high light intensities, when there is a high density of charge carriers. It was hypothesized that the introduction of acceptor nanowires would help lower the amount of recombination under full illumination [71].

A primary challenge with making an all-nanowire active layers has been synthesizing acceptor nanowires of appropriate size, particularly for small molecule acceptors. A series of oligothiophene-functionalized naphthalene diimide (NDI) acceptors were synthesized with varying conjugation length and end groups. Nanowires formed from these compounds were combined with P3HT nanowires to create all-nanowire heterojunctions (Figure 4) [62].

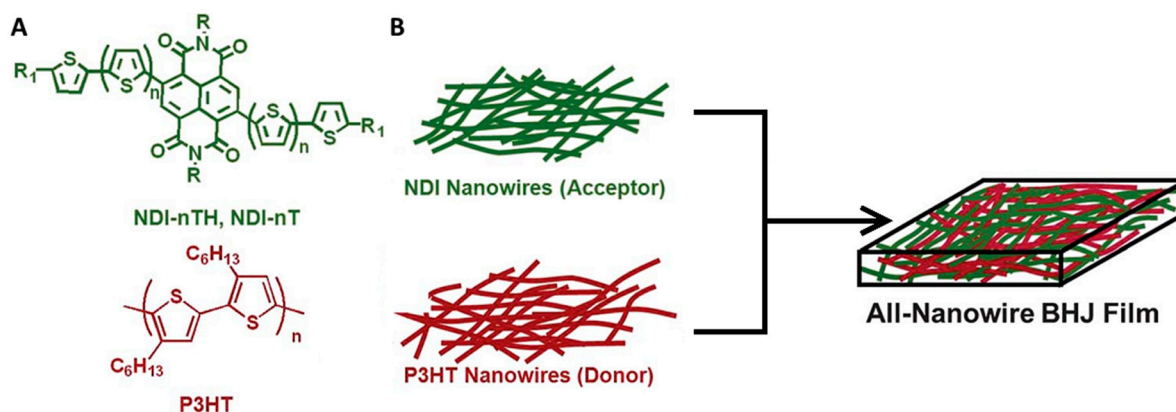


Figure 4. (A) Molecular structure of P3HT and NDI ($n = 1-3$, $R_1 = \text{H}$ or C_6H_{13} , $R = \text{ethylhexyl}$); (B) Schematic of an all-nanowire bulk heterojunction (BHJ) active layer. Adapted from [62] with permission from The Royal Society of Chemistry.

The best performing NDI acceptor had tri-thiophene chains and hexyl end groups (NDI-3TH), providing the narrowest nanoribbons (80–250 nm wide, 14.2–15.3 nm thick, and 2–10 μm long), and the highest V_{oc} , J_{sc} , and FF. When combined with P3HT nanowires, the NDI-3TH wires produced devices with a PCE of 1.15%, 54% greater than optimized bulk-heterojunctions comprising the same molecules [62,72]. This significant increase was attributed to the nanoribbons having narrow domains, which aid in exciton separation, and a bicontinuous network morphology, for effective charge percolation of both electrons and holes.

3.2. Tuning Bulk Heterojunction Domain Size

The creation of appropriately sized domains is of vital importance to OPV performance. If the domains are too large, a large fraction of light-generated excitons will recombine before reaching a donor–acceptor interface where the exciton can be split into free charges. If the domains are too small, then the free charges are less likely to reach the electrodes due to charge trapping.

Although fullerenes have historically outperformed other acceptor molecules, there is significant interest in exploring alternatives [73–78]. Perylene-based dyes have attracted attention due to their

simple synthesis, their low-lying LUMO levels, their light absorption in the visible range, their ability to self-assemble, and their favorable electron transport properties [63,74,79]. Planar perylene diimide (PDI) molecules (Figure 5) have a strong propensity to self-assemble by π - π stacking to form highly crystalline fibers featuring superior electron mobilities [63,79–82]. The dimensions of PDI fibers can be tuned somewhat by altering the processing conditions. However, generally, PDI forms fibers with widths ranging from hundreds of nanometers to several micrometers [63,80,83–92]. When used as an acceptor in bulk heterojunction active layers, PDIs domains are typically too large for efficient exciton separation [93–96], resulting in limited efficiencies [97,98].

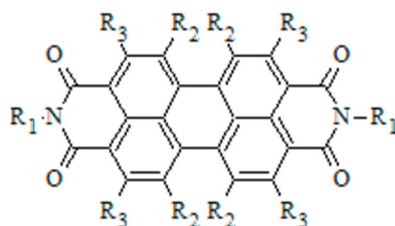


Figure 5. Perylene diimide (PDI) structure with imide (R_1), bay (R_2), and headland (R_3) positions labeled.

One strategy for tuning the assembly of PDI molecules is to alter the amount of lateral offset between the stacked PDI molecules, by adding functional groups such as hexyl, phenethyl, or phenyl groups to the four headland positions (see Figure 6) [99].

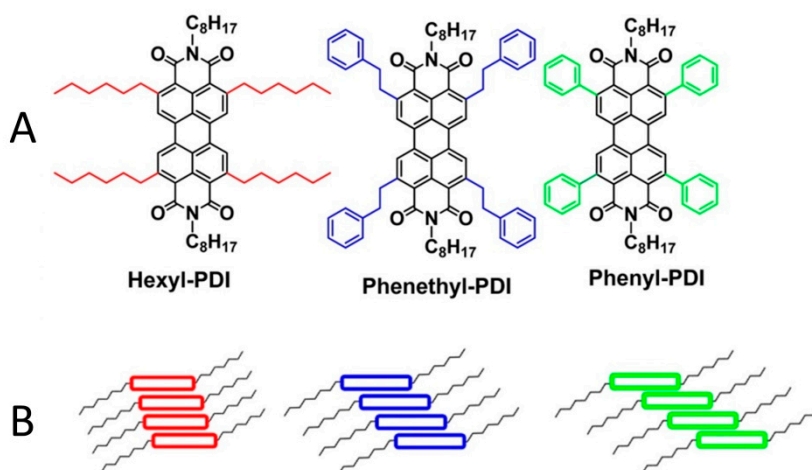


Figure 6. (A) Molecular structure of PDI derivatives and (B) the hypothesized degree of slip-stacking. Adapted from [99] with permission from the American Chemical Society.

In pure films, the hexyl-PDI produced large (1–2 μm) crystalline fibers and the roughest film structure. The phenethyl-PDI formed the smoothest pure film and was the least crystalline. The phenyl-PDI was between the hexyl and phenethyl in terms of crystallinity and roughness of the pure film [99]. A similar trend was observed when these acceptor molecules were blended with polymer donor poly(bithiopheneimide terthiophene) (PBTI3T), though the blend films were smoother and exhibited a reduced crystallinity relative to the pure PDI films. It was the phenyl-PDI-based active layer, and its 2–5 nm crystalline grains, that had the highest J_{sc} and an average PCE of 3.60% [99].

Another approach to mediating the assembly of PDI and limiting PDI domain size in OPV active layers is to form dimers. PDI dimers linked through the imide position have been synthesized, as shown in Figure 7 [100,101]. The PDI moieties are rotated with respect to each other due to the steric repulsion of the imide carbonyls. In blended films with polymer donor poly[4,8-bis-(2-ethylhexyloxy)-benzo[1,2-b:4,5-b']dithiophene-2,6-diyl-alt-4-(2-ethylhexyloxy-1-one)thieno[3,4-b]thiophene-2-yl-2-ethylhexan-1-one] (PDBTTT-CT), PDI monomer domains were several micrometers in size while PDI dimer domains were on the order of 10 nm. A sizeable concurrent increase in OPV performance was obtained, with the J_{sc} increasing from 0.8 to 9.0 mA/cm² and the PCE increasing from 0.13% to 3.20% [100,101].

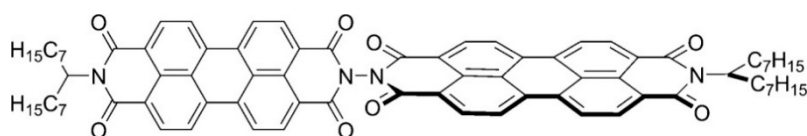


Figure 7. Twisted PDI dimer. Adapted from [100] with permission from the American Chemical Society.

PDI dimers have also been made by attachment at the bay positions. A single covalent link between the monomers allowed for rotation about the bond, which disrupted aggregation. Increasing the number of covalent links between the monomers created more rigid and planar systems that readily aggregate through π -stacking. The reduction in domain size for the singly-linked PDI dimers led to an enhancement of the J_{sc} and a maximum PCE of 3.63% [102].

Very recent studies have used bay-linked PDI dimers to limit the PDI domain size and achieve efficiencies in excess of 6.0% [103,104]. In the best-performing system, a PDI dimer bearing a bulky spiro-fluorene linking group produced domain sizes of 20–30 nm along with a large V_{oc} of 0.98 V when combined with a difluorobenzothiadiazole-quarterthiophene polymer donor, PffBT4T-2DT. It has also been shown that the use of a conjugated fused ring linkage can have similar results due to the combination of domain size reduction and energy level shift [105]. The tunable assembly and concomitant improvements in photovoltaic performance demonstrated with PDI derivatives show great promise for π -stacking acceptor molecules.

3.3. Selective Donor–Acceptor Interactions

Aromatic stacking has also been employed to mediate interactions between donors and acceptors in OPV active layers. As shown in Figure 8, pyrene (Py) groups were attached to a polythiophene to create block copolymers with different ratios of hexyl- and Py-containing blocks [106]. When combined with a Py-containing fullerene derivative (PCBPY) and formed into films using a self-assembly-promoting solvent annealing process, the Py groups of the copolymer and fullerene were able to π -stack, as evidenced by the presence of a new X-ray diffraction peak for the copolymer-fullerene film comprising the 3:1 hexyl:Py copolymer. Transmission electron microscope (TEM) and atomic force microscope (AFM) characterization revealed that as the amount of Py was increased, the morphology changed from one resembling a typical P3HT:PCBM film to a lamellar structure, with 10–20 nm wide domains of alternating PCBPY rich and poor regions [106].

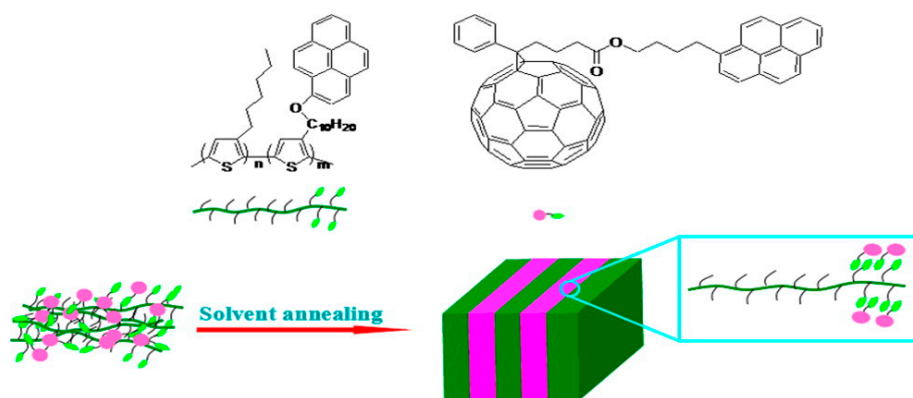


Figure 8. Chemical structures of copolymer donor P3HT-*b*-P3TPy and fullerene acceptor PCPy, and schematic of the self-assembled lamellar active layer structure. Reproduced from [106] with permission from the American Chemical Society.

3.4. Covalently Attached Donors and Acceptors

Another strategy for manipulating the assembly of donor–acceptor systems is to covalently attach donor and acceptor small molecules [107–109], oligomers [110–112], or polymers [113–118]. In some instances, aromatic stacking has led to fibrous coaxial donor–acceptor assemblies [108,115]. When incorporated into organic solar cells, donor–acceptor dyads or copolymers have primarily been used as a third component that can increase the stability of the active layer [114,116], limit macrophase separation, and increase performance [111,113,114,116]. So far, when used as the sole component of an active layer, most covalently attached donor–acceptor systems have exhibited limited OPV performances [109,112,114,117,118].

Recent work with donor–acceptor block copolymers has shown significant promise. When incompatible polymer blocks are covalently linked to form a block copolymer, the blocks phase separate, giving rise to a rich composition-dependent phase behavior that can produce films with lamellar, sphere, cylinder, and gyroid morphologies and tunable nanoscale characteristic lengths [119–121]. Although such nanoscale structuring is highly desirable for organic solar cells, the use of rigid, fully conjugated donor–acceptor block copolymers—for which competition between segregation and crystallization can complicate the self-assembly behavior—are still relatively unexplored [120,122–124].

A fully conjugated block copolymer made from P3HT and a polymer acceptor poly-((9,9-dioctylfluorene)-2,7-diyl-alt-[4,7-bis(thiophen-5-yl)-2,1,3-benzothiadiazole]-2',2''-diyl) (PFTBT) was shown to be close to three times more efficient than a bulk-heterojunction made from the homopolymers; the PCE for the copolymer was 2.7%, compared to 1.0% PCE for the homopolymer blend [125]. The improved performance in the copolymer system was attributed to the lamellar structure of the active layer, the face-on orientation of the copolymer, and the conjugation across the donor–acceptor interface.

Resonant soft X-ray scattering was employed to reveal the lamellar morphology of the active layer, featuring alternating donor and acceptor lamella, oriented normal to the substrate (Figure 9). The width of the individual lamella, about 9 nm, corresponds well with the expected exciton diffusion length, while the vertical orientation of the lamella is well-suited for charge collection. In contrast with the typical edge-on orientation of P3HT in organic solar cell active layers [126–129], the P3HT block of the

copolymer exhibited a preferential face-on orientation, *i.e.*, with the molecular plane nearly parallel to the substrate. It was hypothesized that the preferred orientation of the P3HT resulted from the interaction of the PFTBT with the underlying poly(3,4-ethylenedioxythiophene):polystyrene sulfonate (PEDOT:PSS) hole transport layer [130] which led to a face-on orientation for the PFTBT; since the P3HT was linked to the PFTBT, it adopted a similar orientation [125]. A face-on molecular orientation provides efficient out-of-plane charge transport, along the molecular stacking direction, to the charge collecting electrodes [38,39,53–56]. Finally, the nature of the coupling between donor and acceptor components significantly impacts the exciton dissociation process [131]; in this instance, the conjugated link between the donor and acceptor appears to be more effective at generating charge than the intermolecular interface between donor and acceptor homopolymers.

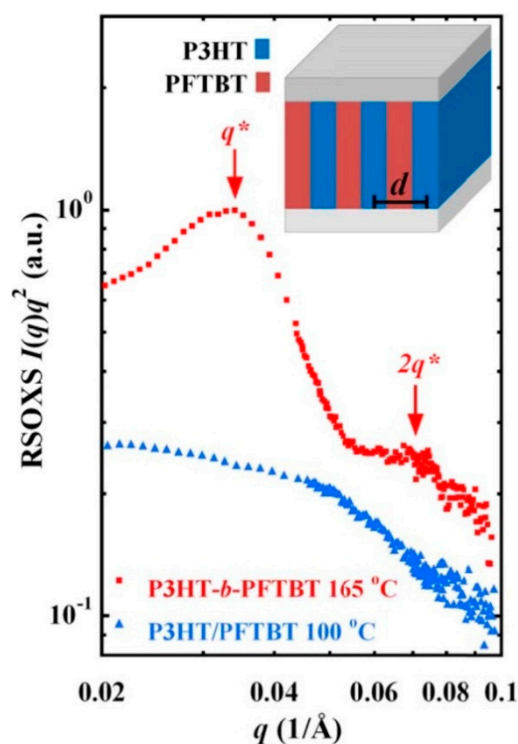


Figure 9. Resonant soft X-ray scattering data showing a well-defined primary scattering peak, q^* , and a weak second-order peak, $2q^*$, indicating the presence of lamellar domains in donor–acceptor block copolymer P3HT-*b*-PFTBT, with a period of $d = 18$ nm. Reproduced from [125] with permission from The American Chemical Society.

4. Hydrogen Bonding

Hydrogen bonding, being a directional and relatively strong supramolecular interaction between hydrogen and polar groups, is promising for mitigating self-assembly. Nature, of course, makes extensive use of hydrogen bonds for generating secondary protein structures, such as alpha helices or beta sheets, and the helical structure of DNA. In this section we discuss the use of hydrogen bonding to mediate self-assembly and stabilize OPV active layers.

4.1. Tuning Self-Assembly with Hydrogen Bonding

In some OPV systems, the donor and acceptor become finely mixed and do not form networks of nanoscale domains that are needed for efficient charge photogeneration and collection. For the thiophene-capped diketopyrrolopyrrole (DPP) small molecule donor shown in Figure 10A, pure DPP films prepared using a stepwise procedure for promoting self-assembly exhibited crystalline grains; however, upon introduction of a fullerene acceptor, phenyl- C_{71} -butyric acid methyl ester ($PC_{71}BM$), DPP assembly was disrupted, resulting in an OPV efficiency of 0.24% [132]. On the other hand, a hairpin-shaped diketopyrrolopyrrole (DPPHP), formed through the covalent attachment of *trans*-1,2-diamidocyclohexane onto DPP, was able to synergistically hydrogen bond and cofacially π -stack to form nanowires (see Figure 10B) [132]. Upon addition of $PC_{71}BM$, the DPP nanowires remained intact, as confirmed by AFM and TEM. Solar cells comprising DPPHP nanowires and $PC_{71}BM$ exhibited an efficiency of 0.53%, more than double that of DPP devices that did not benefit from hydrogen bonding, and 400 times greater than devices in which DPPHP was not induced to self-assemble prior to fullerene addition [132].

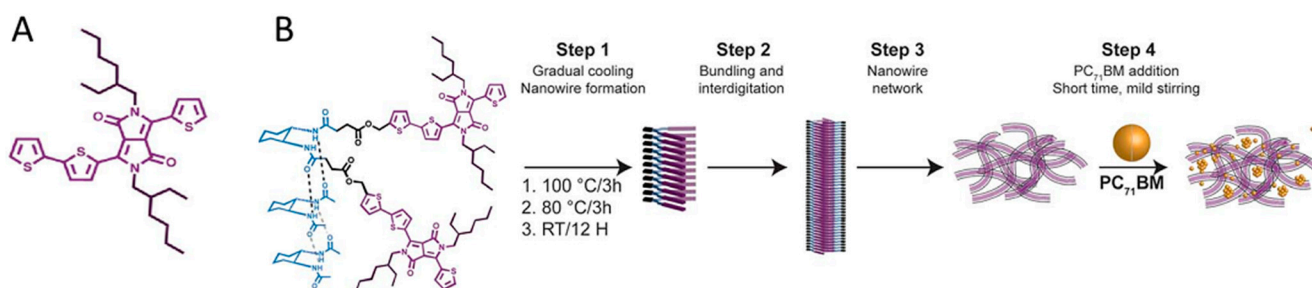


Figure 10. (A) Structure of diketopyrrolopyrrole (DPP); (B) Scheme for generating hydrogen-bonded diketopyrrolopyrrole (DPPHP) nanowires. Adapted from [132] with permission from The Royal Society of Chemistry.

Another study highlights the potential of employing competing π - π and hydrogen bonding interactions for optimizing active layer morphology [133]. Both hydrogen bonding and non-hydrogen bonding DPP compounds, with amide (a-DPP) and ester (e-DPP) side chains, respectively, were synthesized. When blended with $PC_{71}BM$ in films, the e-DPP produced crystalline π -stacked aggregates, about 200 nm in size, while the hydrogen bonding a-DPP maintained a much smaller domain size and a reduced degree of crystallinity. Despite the small domain size and limited molecular order, active layers incorporating the a-DPP had close to twice the hole mobility compared with the e-DPP. This favorable combination of small domain size and efficient charge transport in the a-DPP-based active layer resulted in a dramatically higher J_{sc} , 11.0 mA/cm², compared to 3.9 mA/cm² in the e-DPP, and a PCE of 3.65%. After optimization through the addition of nitrobenzene, the performance of devices comprising a-DPP was further increased to 4.57% PCE owing to an increase in the J_{sc} to 12.6 mA/cm² [133].

The improved performance of the a-DPP was attributed to how the molecule assembled to form short fiber-like interconnected domains, through hydrogen bonding (see Figure 11), that could effectively transport charge. These results support the notion that domain continuity is of paramount important to device performance [134]. The ubiquity of π -interactions in OPV systems opens up the possibility of using competing hydrogen bonding interactions as a general route for disrupting unwanted domain

coarsening [133]. Further work is needed, however, to better predict the conditions under which these intermolecular interactions are competitive or synergistic.

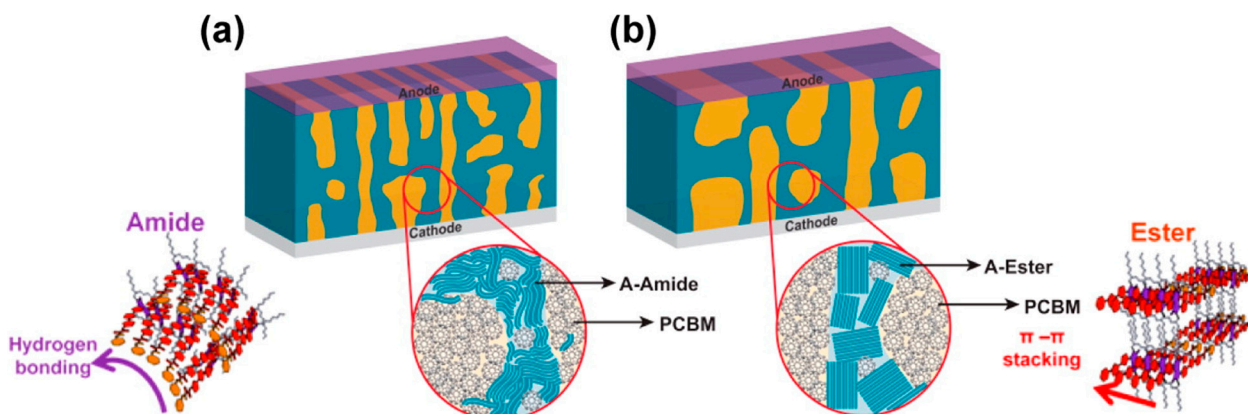


Figure 11. Packing structure and active layer morphology for: (a) amide-DPP; and (b) ester-DPP. Adapted from [133] with permission the American Chemical Society.

4.2. Active Layer Stabilization

For organic solar cells to become a viable technology, the active layer's structure must remain stable under a range of operating conditions. Methods for limiting structural evolution of the active layer are therefore of great importance [50,135–137].

Hydrogen bonding between donor and acceptor has been used to control the distribution and stability of fullerene aggregates in solar cell active layers. An electron donating block copolymer of P3HT-*b*-poly[3-(2,5,8,11-tetraoxadodecane)thiophene] (P3HT-*b*-P3TODT) was synthesized and blended with electron acceptor bisphenyl C₆₁-butyric acid (bis-PCBA), allowing hydrogen bonding to take place between the tetraether sidechain of the P3TODT block and the carboxylic acid of the bis-PCBA [138]. The copolymer formed alternating P3HT and P3TODT lamella in blends comprising up to 40 wt % bis-PCBA. TEM experiments indicated that the bis-PCBA acceptor selectively segregated to the P3TODT regions where hydrogen bonding between the donor and acceptor can take place. This result was supported by the infrared spectra of the blend, which show a shift and a splitting of the carboxylic acid peak, suggesting the presence of hydrogen bonding through a carboxylic acid–ether interaction.

The performance of the P3HT-*b*-P3TODT:bis-PCBA device with hydrogen bonding was twice that of a non-hydrogen bonding P3HT-*b*-P3TODT:PCBM device, but was lower than the P3HT:PCBM reference system, with PCEs of 2.04%, 0.95%, and 3.01%, respectively. Accelerated aging tests, however, showed significant improvements in the stability of the hydrogen bonded system: the P3HT-*b*-P3TODT:bis-PCBA retained 46% of its PCE after being subjected to an elevated temperature of 150 °C for six hours, while the P3HT:PCBM reference device only retained 13% of its PCE under the same conditions. This enhanced stability was attributed to a reduced diffusion of the fullerene due to the fullerene being hydrogen bonded to the copolymer donor [138].

In another study looking to increase stability, a “three-point” complementary hydrogen bonding scheme was employed, in which three hydrogen bonds are simultaneously formed between donor and acceptor [139–141]. Using a polythiophene block copolymer functionalized with isoorotic acid (P3HT-*b*-P3IOA) and diaminopyridine tethered fullerene derivative (PCBP) shown in Figure 12 [141],

it was found that bulk heterojunction devices with the hydrogen-bonded derivatives were highly resistant to structural change, as evidenced by accelerated aging tests, done at 110 °C for 112 h [139]. The non-hydrogen bonding P3HT:PCBM reference device retained less than 40% of its PCE, while devices that incorporated components that were able to form one (P3HT-*b*-P3IOA:PCBM) or three (P3HT-*b*-P3IOA:PCBP) hydrogen bonds retained 65% and 75% of their initial PCE, respectively.

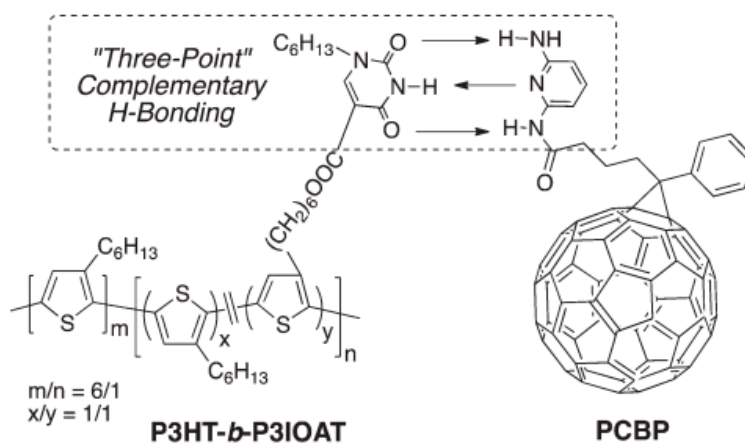


Figure 12. Structure of copolymer donor P3HT-*b*-P3IOA and fullerene acceptor PCBP, along with the three-point hydrogen bonding between the compounds. Reproduced from [141] with permission from The Royal Society of Chemistry.

In a follow-up study, P3HT-*b*-P3IOA nanowires were formed through solvent-induced precipitation [140]. The addition of fullerene acceptor PCBP led to an increase in the nanowire diameter, indicating that the PCBP was hydrogen bonding to P3HT-*b*-P3IOA at the surface of the nanowire to generate a core-shell structure. When compared with active layers comprised of P3HT nanowires and PCBM, the copolymer system exhibited a significant reduction in the proportion of edge-on-oriented molecules, *i.e.*, fewer molecules were oriented with the molecular plane nearly perpendicular to the substrate. This difference in molecular orientation between the two systems was attributed to the difference in the side-chain interaction with the PEDOT:PSS substrate [141]. A reduction in the proportion of edge-on oriented molecules is expected to facilitate out-of-plane charge transport to the anode and cathode [38,55,56,126,127,142–146]. When subjected to accelerated aging, the hydrogen bonded nanowire system was more stable, retaining 80% of the PCE after 112 h at 110 °C while the reference nanowire P3HT:PCBM device retained only 60% of its PCE after the same treatment [140].

4.3. Molecular Additives

Certain molecular additives have been shown to effectively promote the formation of nanostructured active layers, while simplifying device fabrication, *e.g.*, circumventing the need for annealing [116,147–151]. 2,3-Pyridinediol is an interesting case, as it can hydrogen bond with the ester of PCBM while also π -stacking with the P3HT backbone [152]. This additive was found to increase the photovoltaic performance of P3HT:PCBM solar cells and allow for the use of relatively thick active layer films (350 nm). These improvements were associated with the presence of bicontinuous donor and acceptor nanodomains, about 30 nm in width, and an altered distribution of P3HT and PCBM throughout

the active layer. Interfacial segregation during active layer formation commonly leads to a gradient in the proportion of donor and acceptor at different film depths [153–155]. In bulk-heterojunction P3HT:PCBM active layers, the top surface can consist of P3HT concentrations as high as 97 wt % [153–156]. As shown in Figure 13, addition of 2,3-pyridinediol led to a more evenly distributed vertical composition measured by X-ray photoelectron spectroscopy (XPS), with the sulfur content being representative of the P3HT, the oxygen of the PCBM, and the nitrogen of the 2,3-pyridinediol itself [152]. A more uniform distribution of donor and acceptor throughout the depth of the film is expected to lead to improved charge percolation.

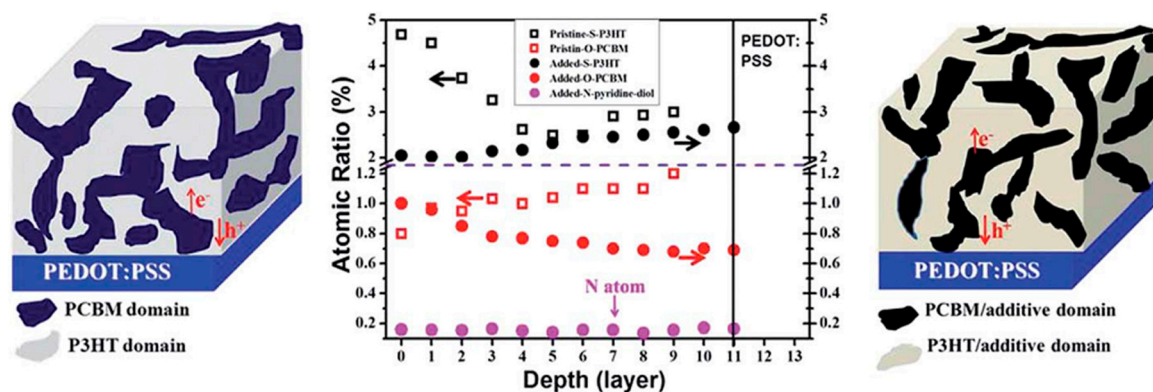


Figure 13. XPS Depth profile analysis of unannealed P3HT:PCBM films with and without additive. Reproduced from [152] with permission from The Royal Society of Chemistry.

The same additive was also effective for boosting the efficiency of P3HT:indene- C_{60} bisadduct and PTB7:PC $_{71}$ BM OPV devices with their respective PCE increasing from 3.35% to 5.93% and 5.46% to 7.54%, without and with the additive [152]. Furthermore, 2,3-pyridinediol led to improved device stability relative to the more commonly used additive 1,8-diiodooctane (DIO) in the PTB7:PC $_{71}$ BM device, with only a 3% drop in PCE, from 7.54% to 7.30%, after heating at 100 °C for 30 minutes, relative to a 36% drop in PCE, from 6.62% to 4.26%, for DIO.

5. Shape Complementarity

Shape complementarity is the principle of combining geometrically complementary molecules. This approach can be used to generate interlocking assemblies with intimate contact between donor and acceptor.

Contorted hexabenzocoronenes (c-HBC) have been combined with fullerenes, to produce ball-and-socket assemblies, as depicted in Figure 14 [157]. XPS measurements show the carbon 1s peak shifting to higher energy, and narrowing, which is consistent with improved charge transfer at the donor–acceptor interface. This improved charge transfer drives an enhancement in performance: c-HBC: C_{60} devices exhibit an efficiency that is 14 times greater than devices comprised of flat HBC analogues [157], while devices comprising contorted dibenzotetrathienocoronenes (DBTTC) and C_{60} have produced a PCE as high as 2.7% [158]. This efficiency is remarkable considering that neither the c-HBC nor the C_{60} absorb light appreciably in the visible wavelength range. This type of transparent solar cell has exciting potential for integration into light-harvesting windows. Other types of shape matching systems with potential applications for OPVs are also gaining attention, such as the buckycatchers shown in Figure 15 [159–161].

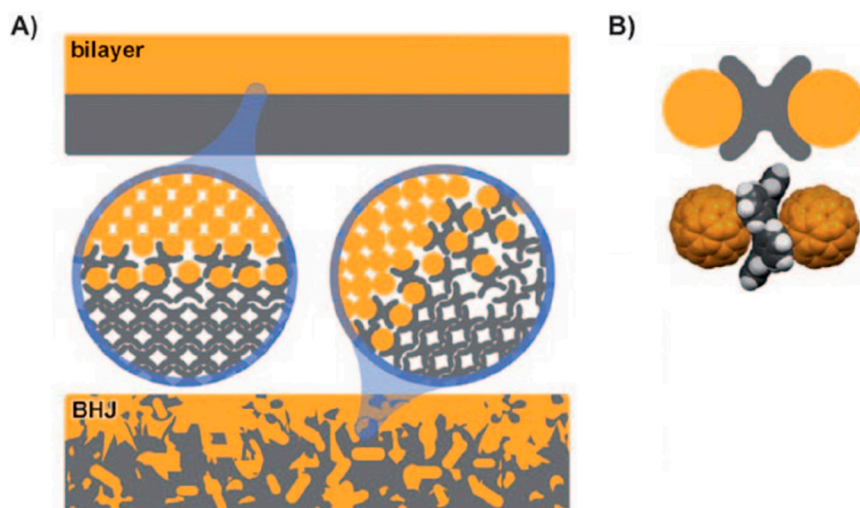


Figure 14. (A) Depiction of ball-and-socket interfaces in bilayer and bulk-heterojunction devices; (B) schematic depiction and molecular structure of the interface between c-HBC and C₆₀. Adapted from [157] with permission from John Wiley and Sons.

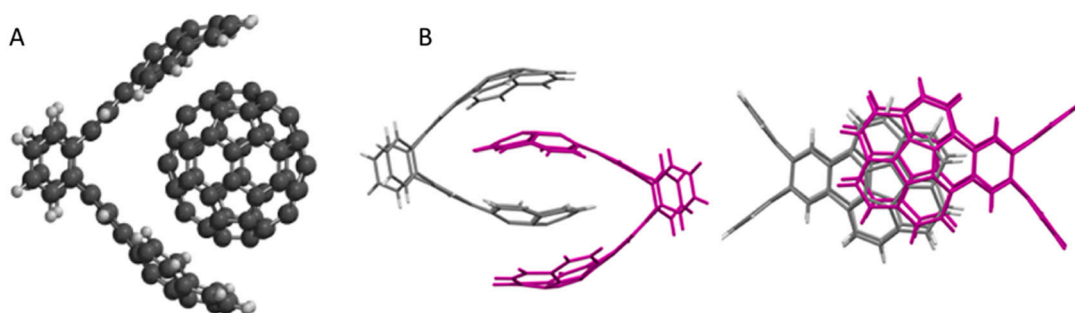


Figure 15. (A) Concave-concave buckycatcher around C₆₀; (B) Interdigitated concave-concave buckycatchers. Adapted from [161] with permission from the American Chemical Society.

6. Conclusions

Supramolecular interactions are an effective tool for tuning the nanoscale morphology of OPV active layers and improving OPV performance. Nanowires formed through aromatic stacking exhibit narrow domains that benefit charge photogeneration and provide continuous pathways for charge collection, while allowing for the use of thicker active layers that absorb more light. Limiting the self-assembly of π -stacking small molecules through the addition of side chains, or the formation of dimers, has been effective for tuning domain size, resulting in some of the highest documented efficiencies for non-fullerene acceptors. Block copolymers have also been used to assemble appropriately-sized donor and acceptor domains with an alternating lamellar arrangement. Hydrogen bonding was shown to be effective for mediating interactions between OPV components, while simultaneously making the active layer more resistant to structural change during accelerated aging tests. Moreover, shape complementarity enabled performance improvements through intimate interfacial contact between donor and acceptor. Taken together, these results show the tremendous promise of supramolecular approaches for tailoring organic solar cell active structure with unprecedented control and predictability.

Acknowledgments

The authors acknowledge support from the Binghamton University Smart Energy Transdisciplinary Area of Excellence Collaboration Grants Program.

Author Contributions

Alexander M. Haruk and Jeffrey M. Mativetsky wrote and revised the paper.

Conflicts of Interest

The authors declare no conflict of interest.

References

1. Dennler, G.; Scharber, M.C.; Brabec, C.J. Polymer-fullerene bulk-heterojunction solar cells. *Adv. Mater.* **2009**, *21*, 1323–1338.
2. Scharber, M.C.; Sariciftci, N.S. Efficiency of bulk-heterojunction organic solar cells. *Prog. Polym. Sci.* **2013**, *38*, 1929–1940.
3. Mazzi, K.A.; Luscombe, C.K. The future of organic photovoltaics. *Chem. Soc. Rev.* **2014**, *44*, 78–90.
4. Lyons, B.P.; Clarke, N.; Groves, C. The relative importance of domain size, domain purity and domain interfaces to the performance of bulk-heterojunction organic photovoltaics. *Energy Environ. Sci.* **2012**, *5*, 7657–7663.
5. Darling, S.B.; You, F. The case for organic photovoltaics. *RSC Adv.* **2013**, *3*, 17633–17648.
6. Hoppe, H.; Sariciftci, N.S. Organic solar cells: An overview. *J. Mater. Res.* **2004**, *19*, 1924–1945.
7. Servaites, J.D.; Ratner, M.A.; Marks, T.J. Organic solar cells: A new look at traditional models. *Energy Environ. Sci.* **2011**, *4*, 4410–4422.
8. Walker, B.; Kim, C.; Nguyen, T.-Q. Small molecule solution—Processed bulk heterojunction solar cells. *Chem. Mater.* **2011**, *23*, 470–482.
9. Krebs, F.C. Fabrication and processing of polymer solar cells: A review of printing and coating techniques. *Sol. Energy Mater. Sol. Cells* **2009**, *93*, 394–412.
10. Krebs, F.C.; Tromholt, T.; Jørgensen, M. Upscaling of polymer solar cell fabrication using full roll-to-roll processing. *Nanoscale* **2010**, *2*, 873–886.
11. He, Z.; Xiao, B.; Liu, F.; Wu, H.; Yang, Y.; Xiao, S.; Wang, C.; Russell, T.P.; Cao, Y. Single-junction polymer solar cells with high efficiency and photovoltage. *Nat. Photonics* **2015**, *9*, 174–179.
12. Liu, Y.; Zhao, J.; Li, Z.; Mu, C.; Ma, W.; Hu, H.; Jiang, K.; Lin, H.; Ade, H.; Yan, H. Aggregation and morphology control enables multiple cases of high-efficiency polymer solar cells. *Nat. Commun.* **2014**, *5*, 5293.
13. Chen, C.C.; Chang, W.H.; Yoshimura, K.; Ohya, K.; You, J.; Gao, J.; Hong, Z.; Yang, Y. An efficient triple-junction polymer solar cell having a power conversion efficiency exceeding 11%. *Adv. Mater.* **2014**, *26*, 5670–5677.

14. Yan, J.; Saunders, B.R. Third-generation solar cells: A review and comparison of polymer: Fullerene, hybrid polymer and perovskite solar cells. *RSC Adv.* **2014**, *4*, 43286–43314.
15. Nagarjuna, G.; Venkataraman, D. Strategies for controlling the active layer morphologies in OPVs. *J. Polym. Sci. B* **2012**, *50*, 1045–1056.
16. Alam, M.A.; Ray, B.; Khan, M.R.; Dongaonkar, S. The essence and efficiency limits of bulk-heterostructure organic solar cells: A polymer-to-panel perspective. *J. Mater. Res.* **2013**, *28*, 541–557.
17. Müller-Buschbaum, P. The active layer morphology of organic solar cells probed with grazing incidence scattering techniques. *Adv. Mater.* **2014**, *26*, 7692–7709.
18. Tsoi, W.C.; Nicholson, P.G.; Kim, J.S.; Roy, D.; Burnett, T.L.; Murphy, C.E.; Nelson, J.; Bradley, D.D.C.; Kim, J.-S.; Castro, F.A. Surface and subsurface morphology of operating nanowire: Fullerene solar cells revealed by photoconductive-AFM. *Energy Environ. Sci.* **2011**, *4*, 3646–3651.
19. Vakhshouri, K.; Kesava, S.V.; Kozub, D.R.; Gomez, E.D. Characterization of the mesoscopic structure in the photoactive layer of organic solar cells: A focused review. *Mater. Lett.* **2013**, *90*, 97–102.
20. Giridharagopal, R.; Ginger, D.S. Characterizing morphology in bulk heterojunction organic photovoltaic systems. *J. Phys. Chem. Lett.* **2010**, *1*, 1160–1169.
21. DeLongchamp, D.M.; Kline, R.J.; Herzog, A. Nanoscale structure measurements for polymer-fullerene photovoltaics. *Energy Environ. Sci.* **2012**, *5*, 5980–5993.
22. Brady, M.A.; Su, G.M.; Chabynyc, M.L. Recent progress in the morphology of bulk heterojunction photovoltaics. *Soft Matter* **2011**, *7*, 11065–11077.
23. Liang, Y.; Wang, H.; Yuan, S.; Lee, Y.; Gan, L.; Yu, L. Conjugated block copolymers and co-oligomers: From supramolecular assembly to molecular electronics. *J. Mater. Chem.* **2007**, *17*, 2183–2194.
24. Babu, S.S.; Möhwald, H.; Nakanishi, T. Recent progress in morphology control of supramolecular fullerene assemblies and its applications. *Chem. Soc. Rev.* **2010**, *39*, 4021–4035.
25. Hoeben, F.J.M.; Jonkheijm, P.; Meijer, E.W.; Schenning, A.P.H.J. About supramolecular assemblies of π -conjugated systems. *Chem. Rev.* **2005**, *105*, 1491–1546.
26. Ciesielski, A.; Palma, C.A.; Bonini, M.; Samori, P. Towards supramolecular engineering of functional nanomaterials: Pre-programming multi-component 2D self-assembly at solid-liquid interfaces. *Adv. Mater.* **2010**, *22*, 3506–3520.
27. Elemans, J.A.A.W.; Lei, S.; de Feyter, S. Molecular and supramolecular networks on surfaces: From two-dimensional crystal engineering to reactivity. *Angew. Chem. Int. Ed.* **2009**, *48*, 7298–7333.
28. Kondratuk, D.V.; Perdigão, L.M.A.; Esmail, A.M.S.; O’Shea, J.N.; Beton, P.H.; Anderson, H.L. Supramolecular nesting of cyclic polymers. *Nat. Chem.* **2015**, *7*, 317–322.
29. Bruni, F.; Sassi, M.; Campione, M.; Giovanella, U.; Ruffo, R.; Luzzati, S.; Meinardi, F.; Beverina, L.; Brovelli, S. Post-deposition activation of latent hydrogen-bonding: A new paradigm for enhancing the performances of bulk heterojunction solar cells. *Adv. Funct. Mater.* **2014**, *24*, 7410–7419.

30. Kim, F.S.; Ren, G.; Jenekhe, S.A. One-dimensional nanostructures of π -conjugated molecular systems: Assembly, properties, and applications from photovoltaics, sensors, and nanophotonics to nanoelectronics. *Chem. Mater.* **2011**, *23*, 682–732.
31. Yu, G.; Gao, J.; Hummelen, J.C.; Wudl, F.; Heeger, A.J. Polymer photovoltaic cells: Enhanced efficiencies via a network of internal donor–acceptor heterojunctions. *Science* **1995**, *270*, 1789–1791.
32. Collins, B.A.; Gann, E.; Guignard, L.; He, X.; McNeill, C.R.; Ade, H. Molecular miscibility of polymer–fullerene blends. *J. Phys. Chem. Lett.* **2010**, *1*, 3160–3166.
33. Treat, N.D.; Varotto, A.; Takacs, C.J.; Batarra, N.; Al-Hashimi, M.; Heeney, M.J.; Heeger, A.J.; Wudl, F.; Hawker, C.J.; Chabynyc, M.L. Polymer–fullerene miscibility: A metric for screening new materials for high-performance organic solar cells. *J. Am. Chem. Soc.* **2012**, *134*, 15869–15879.
34. Miller, N.C.; Cho, E.; Gysel, R.; Risko, C.; Coropceanu, V.; Miller, C.E.; Sweetnam, S.; Sellinger, A.; Heeney, M.; McCulloch, I.; *et al.* Factors governing intercalation of fullerenes and other small molecules between the side chains of semiconducting polymers used in solar cells. *Adv. Energy Mater.* **2012**, *2*, 1208–1217.
35. Bartelt, J.A.; Beiley, Z.M.; Hoke, E.T.; Mateker, W.R.; Douglas, J.D.; Collins, B.A.; Tumbleston, J.R.; Graham, K.R.; Amassian, A.; Ade, H.; *et al.* The importance of fullerene percolation in the mixed regions of polymer–fullerene bulk heterojunction solar cells. *Adv. Energy Mater.* **2013**, *3*, 364–374.
36. Coropceanu, V.; Cornil, J.; da Silva Filho, D.A.; Olivier, Y.; Silbey, R.; Bredas, J.-L. Charge transport in organic semiconductors. *Chem. Rev.* **2007**, *107*, 926–952.
37. Mas-Torrent, M.; Rovira, C. Role of molecular order and solid-state structure in organic field-effect transistors. *Chem. Rev.* **2011**, *111*, 4833–4856.
38. Mativetsky, J.M.; Wang, H.; Lee, S.S.; Whittaker-Brooks, L.; Loo, Y.-L. Face-on stacking and enhanced out-of-plane hole mobility in graphene-templated copper phthalocyanine. *Chem. Commun.* **2014**, *50*, 5319–5321.
39. Geng, Y.; Wu, S.-X.; Li, H.-B.; Tang, X.-D.; Wu, Y.; Su, Z.-M.; Liao, Y. A theoretical discussion on the relationships among molecular packings, intermolecular interactions, and electron transport properties for naphthalene tetracarboxylic diimide derivatives. *J. Mater. Chem.* **2011**, *21*, 15558–15566.
40. Olivier, Y.; Lemaire, V.; Brédas, J.L.; Cornil, J. Charge hopping in organic semiconductors: Influence of molecular parameters on macroscopic mobilities in model one-dimensional stacks. *J. Phys. Chem. A* **2006**, *110*, 6356–6364.
41. Facchetti, A. π -Conjugated polymers for organic electronics and photovoltaic cell applications. *Chem. Mater.* **2011**, *23*, 733–758.
42. Gershenson, M.E.; Podzorov, V.; Morpurgo, A.F. Colloquium: Electronic transport in single-crystal organic transistors. *Rev. Mod. Phys.* **2006**, *78*, 973–989.
43. Pfattner, R.; Mas-Torrent, M.; Bilotti, I.; Brillante, A.; Milita, S.; Liscio, F.; Biscarini, F.; Marszalek, T.; Ulanski, J.; Nosal, A.; *et al.* High-performance single crystal organic field-effect transistors based on two dithiophene-tetrathiafulvalene (DT-TTF) polymorphs. *Adv. Mater.* **2010**, *22*, 4198–4203.

44. Lee, S.S.; Mativetsky, J.M.; Loth, M.A.; Anthony, J.E.; Loo, Y.L. Quantifying resistances across nanoscale low- and high-angle interspherulite boundaries in solution-processed organic semiconductor thin films. *ACS Nano* **2012**, *6*, 9879–9886.
45. Hiszpanski, A.M.; Baur, R.M.; Kim, B.; Tremblay, N.J.; Nuckolls, C.; Woll, A.R.; Loo, Y. Tuning polymorphism and orientation in organic semiconductor thin films via post-deposition processing. *J. Am. Chem. Soc.* **2014**, *136*, 15749–15756.
46. Etxebarria, I.; Ajuria, J.; Pacios, R. Polymer: Fullerene solar cells: Materials, processing issues, and cell layouts to reach power conversion efficiency over 10%, a review. *J. Photonics Energy* **2015**, *5*, 057214.
47. Marsh, R.A.; Groves, C.; Greenham, N.C. A microscopic model for the behavior of nanostructured organic photovoltaic devices. *J. Appl. Phys.* **2007**, *101*, 083509.
48. Gadisa, A.; Svensson, M.; Andersson, M.R.; Inganäs, O. Correlation between oxidation potential and open-circuit voltage of composite solar cells based on blends of polythiophenes/fullerene derivative. *Appl. Phys. Lett.* **2004**, *84*, 1609–1611.
49. Brabec, C.J.; Cravino, A.; Meissner, D.; Serdar Sariciftci, N.; Fromherz, T.; Rispen, M.T.; Sanchez, L.; Hummelen, J.C. Origin of the open circuit voltage of plastic solar cells. *Adv. Funct. Mater.* **2001**, *11*, 374–380.
50. Brabec, C.J.; Gowrisanker, S.; Halls, J.J.M.; Laird, D.; Jia, S.; Williams, S.P. Polymer-fullerene bulk-heterojunction solar cells. *Adv. Mater.* **2010**, *22*, 3839–3856.
51. Liao, H.C.; Ho, C.C.; Chang, C.Y.; Jao, M.H.; Darling, S.B.; Su, W.F. Additives for morphology control in high-efficiency organic solar cells. *Mater. Today* **2013**, *16*, 326–336.
52. Chu, C.-W.; Yang, H.; Hou, W.-J.; Huang, J.; Li, G.; Yang, Y. Control of the nanoscale crystallinity and phase separation in polymer solar cells. *Appl. Phys. Lett.* **2008**, *92*, 103306.
53. Kim, D.H.; Lee, D.Y.; Lee, H.S.; Lee, W.H.; Kim, Y.H.; Han, J.I.; Cho, K. High-mobility organic transistors based on single-crystalline microribbons of triisopropylsilylethynyl pentacene via solution-phase self-assembly. *Adv. Mater.* **2007**, *19*, 678–682.
54. Reese, C.; Bao, Z. High-resolution measurement of the anisotropy of charge transport in single crystals. *Adv. Mater.* **2007**, *19*, 4535–4538.
55. Anthony, J.E.; Brooks, J.S.; Eaton, D.L.; Parkin, S.R. Functionalized pentacene: Improved electronic properties from control of solid-state order. *J. Am. Chem. Soc.* **2001**, *123*, 9482–9483.
56. Sundar, V.C.; Zaumseil, J.; Podzorov, V.; Menard, E.; Willett, R.L.; Someya, T.; Gershenson, M.E.; Rogers, J.A. Elastomeric transistor stamps: Transport in organic crystals. *Science* **2004**, *303*, 1644–1646.
57. Kim, J.S.; Lee, J.H.; Park, J.H.; Shim, C.; Sim, M.; Cho, K. High-efficiency organic solar cells based on preformed poly(3-hexylthiophene) nanowires. *Adv. Funct. Mater.* **2011**, *21*, 480–486.
58. Jo, S.B.; Lee, W.H.; Qiu, L.; Cho, K. Polymer blends with semiconducting nanowires for organic electronics. *J. Mater. Chem.* **2012**, *22*, 4244–4260.
59. Ren, G.; Wu, P.-T.; Jenekhe, S.A. Solar cells based on block copolymer semiconductor nanowires: Effects of nanowire aspect ratio. *ACS Nano* **2011**, *5*, 376–384.
60. Kim, J.-H.; Kim, M.; Jinnai, H.; Shin, T.J.; Kim, H.; Park, J.H.; Jo, S.B.; Cho, K. Organic solar cells based on three-dimensionally percolated polythiophene nanowires with enhanced charge transport. *ACS Appl. Mater. Interfaces* **2014**, *6*, 5640–5650.

61. Kim, J.S.; Park, Y.; Lee, D.Y.; Lee, J.H.; Park, J.H.; Kim, J.K.; Cho, K. Poly(3-hexylthiophene) nanorods with aligned chain orientation for organic photovoltaics. *Adv. Funct. Mater.* **2010**, *20*, 540–545.
62. Ren, G.; Ahmed, E.; Jenekhe, S.A. Nanowires of oligothiophene-functionalized naphthalene diimides: Self assembly, morphology, and all-nanowire bulk heterojunction solar cells. *J. Mater. Chem.* **2012**, *22*, 24373–24379.
63. Briseno, A.L.; Mannsfeld, S.C.B.; Reese, C.; Hancock, J.M.; Xiong, Y.; Jenekhe, S.A.; Bao, Z.; Xia, Y. Perylenediimide nanowires and their use in fabricating field-effect transistors and complementary inverters. *Nano Lett.* **2007**, *7*, 2847–2853.
64. Kim, M.; Kim, J.-H.; Choi, H.H.; Park, J.H.; Jo, S.B.; Sim, M.; Kim, J.S.; Jinnai, H.; Park, Y.D.; Cho, K. Electrical performance of organic solar cells with additive-assisted vertical phase separation in the photoactive layer. *Adv. Energy Mater.* **2014**, *4*, 1300612.
65. Mativetsky, J.M.; Orgiu, E.; Lieberwirth, I.; Pisula, W.; Samori, P. Charge transport over multiple length scales in supramolecular fiber transistors: Single fiber *versus* ensemble performance. *Adv. Mater.* **2014**, *26*, 430–435.
66. Koster, L.J.A.; Mihailetchi, V.D.; Xie, H.; Blom, P.W.M. Origin of the light intensity dependence of the short-circuit current of polymer/fullerene solar cells. *Appl. Phys. Lett.* **2005**, *87*, 203502.
67. Mihailetchi, V.D.; Wildeman, J.; Blom, P.W.M. Space-charge limited photocurrent. *Phys. Rev. Lett.* **2005**, *94*, 126602.
68. Ooi, Z.E.; Chan, K.L.; Lombardo, C.J.; Dodabalapur, A. Analysis of photocurrents in lateral-geometry organic bulk heterojunction devices. *Appl. Phys. Lett.* **2012**, *101*, 053301.
69. Briseno, A.L.; Holcombe, T.W.; Boukai, A.I.; Garnett, E.C.; Shelton, S.W.; Fréchet, J.J.M.; Yang, P. Oligo- and polythiophene/ZnO hybrid nanowire solar cells. *Nano Lett.* **2010**, *10*, 334–340.
70. Kim, K.; Shin, J.W.; Lee, Y.B.; Cho, M.Y.; Lee, S.H.; Park, D.H.; Jang, D.K.; Lee, C.J.; Joo, J. Poly(3-hexylthiophene)/multiwalled carbon hybrid coaxial nanotubes: Nanoscale rectification and photovoltaic characteristics. *ACS Nano* **2010**, *4*, 4197–4205.
71. Kim, M.; Park, J.H.; Kim, J.H.; Sung, J.H.; Jo, S.B.; Jo, M.-H.; Cho, K. Lateral organic solar cells with self-assembled semiconductor nanowires. *Adv. Energy Mater.* **2014**, *5*, 1401317.
72. Ren, G.; Ahmed, E.; Jenekhe, S.A. Non-fullerene acceptor-based bulk heterojunction polymer solar cells: Engineering the nanomorphology via processing additives. *Adv. Energy Mater.* **2011**, *1*, 946–953.
73. Anthony, J.E. Small-molecule, nonfullerene acceptors for polymer bulk heterojunction organic photovoltaics. *Chem. Mater.* **2011**, *23*, 583–590.
74. Huang, C.; Barlow, S.; Marder, S.R. Perylene-3,4,9,10-tetracarboxylic acid diimides: Synthesis, physical properties, and use in organic electronics. *J. Org. Chem.* **2011**, *76*, 2386–2407.
75. Zhang, F.; Brandt, R.G.; Gu, Z.; Wu, S.; Andersen, T.R.; Shi, M.; Yu, D.; Chen, H. The effect of molecular geometry on the photovoltaic property of diketopyrrolopyrrole based non-fullerene acceptors. *Synth. Met.* **2015**, *203*, 249–254.
76. Wu, J.; Ma, Y.; Wu, N.; Lin, Y.; Lin, J.; Wang, L.; Ma, C.-Q. 2,2-Dicyanovinyl-end-capped oligothiophenes as electron acceptor in solution processed bulk-heterojunction organic solar cells. *Org. Electron.* **2015**, *23*, 28–38.

77. Liu, W.; Shi, H.; Andersen, T.R.; Zawacka, N.K.; Cheng, P.; Bundgaard, E.; Shi, M.; Zhan, X.; Krebs, F.C.; Chen, H. Roll-coating fabrication of ITO-free flexible solar cells based on a non-fullerene small molecule acceptor. *RSC Adv.* **2015**, *5*, 36001–36006.
78. Sherman, J.B.; Purushothaman, B.; Parkin, S.R.; Kim, C.; Collins, S.; Anthony, J.; Nguyen, T.-Q.; Chabinyc, M.L. Role of crystallinity of non-fullerene acceptors in bulk heterojunctions. *J. Mater. Chem. A* **2015**, *3*, 9989–9998.
79. Abhijith, T.; Ameen, M.Y.; Reddy, V.S. Synthesis of PTCDI-C 8 one dimensional nanostructures for photovoltaic applications. *IOP Conf. Ser. Mater. Sci. Eng.* **2015**, *73*, 012052.
80. Savage, R.C.; Orgiu, E.; Mativetsky, J.M.; Pisula, W.; Schnitzler, T.; Eversloh, C.L.; Li, C.; Müllen, K.; Samorì, P. Charge transport in fibre-based perylene-diimide transistors: Effect of the alkyl substitution and processing technique. *Nanoscale* **2012**, *4*, 2387–2393.
81. Ostrick, J.R.; Dodabalapur, A.; Torsi, L.; Lovinger, A.J.; Kwock, E.W.; Miller, T.M.; Galvin, M.; Berggren, M.; Katz, H.E. Conductivity-type anisotropy in molecular solids. *J. Appl. Phys.* **1997**, *81*, 6804–6808.
82. Malenfant, P.R.L.; Dimitrakopoulos, C.D.; Gelorme, J.D.; Kosbar, L.L.; Graham, T.O.; Curioni, A.; Andreoni, W. *N*-type organic thin-film transistor with high field-effect mobility based on a *N,N'*-dialkyl-3,4,9,10-perylene tetracarboxylic diimide derivative. *Appl. Phys. Lett.* **2002**, *80*, 2517–2519.
83. Liscio, A.; de Luca, G.; Nolde, F.; Palermo, V.; Müllen, K.; Samorì, P. Photovoltaic charge generation visualized at the nanoscale: A proof of principle. *J. Am. Chem. Soc.* **2008**, *130*, 780–781.
84. Dittmer, J.J.; Lazzaroni, R.; Leclere, P.; Moretti, P.; Granstrom, M.; Petritsch, K.; Marseglia, E.A.; Friend, R.H.; Bredas, J.L.; Rost, H.; *et al.* Crystal network formation in organic solar cells. *Sol. Energy Mater. Sol. Cells* **2000**, *61*, 53–61.
85. Oh, J.H.; Liu, S.; Bao, Z.; Schmidt, R.; Würthner, F. Air-stable *N*-channel organic thin-film transistors with high field-effect mobility based on *N,N'*-bis(heptafluorobutyl)-3,4,9,10-perylene diimide. *Appl. Phys. Lett.* **2007**, *91*, 123–126.
86. Chen, H.Z.; Ling, M.M.; Mo, X.; Shi, M.M.; Wang, M.; Bao, Z. Air stable *N*-channel organic semiconductors for thin film transistors based on fluorinated derivatives of perylene diimides. *Chem. Mater.* **2007**, *19*, 816–824.
87. De Luca, G.; Treossi, E.; Liscio, A.; Mativetsky, J.M.; Scolaro, L.M.; Palermo, V.; Samorì, P. Solvent vapour annealing of organic thin films: Controlling the self-assembly of functional systems across multiple length scales. *J. Mater. Chem.* **2010**, *20*, 2493–2498.
88. Datar, A.; Oitker, R.; Zang, L. Surface-assisted one-dimensional self-assembly of a perylene based semiconductor molecule. *Chem. Commun.* **2006**, 1649–1651.
89. Balakrishnan, K.; Datar, A.; Naddo, T.; Huang, J.; Oitker, R.; Yen, M.; Zhao, J.; Zang, L. Effect of side-chain substituents on self-assembly of perylene diimide molecules: Morphology control. *J. Am. Chem. Soc.* **2006**, *128*, 7390–7398.
90. Balakrishnan, K.; Datar, A.; Oitker, R.; Chen, H.; Zuo, J.; Zang, L. Nanobelt self-assembly from an organic *N*-type semiconductor: Propoxyethyl-PTCDI. *J. Am. Chem. Soc.* **2005**, *127*, 10496–10497.
91. Zang, L.; Che, Y.; Moore, J.S. One-dimensional self-assembly of planar π -conjugated molecules: Adaptable building blocks for organic nanodevices. *Acc. Chem. Res.* **2008**, *41*, 1596–1608.

92. Palermo, V.; Liscio, A.; Gentilini, D.; Nolde, F.; Müllen, K.; Samori, P. Scanning probe microscopy investigation of self-organized perylenetetracarboxydiimide nanostructures at surfaces: Structural and electronic properties. *Small* **2007**, *3*, 161–167.
93. Engel, E.; Leo, K.; Hoffmann, M. Ultrafast relaxation and exciton-exciton annihilation in PTCDA thin films at high excitation densities. *Chem. Phys.* **2006**, *325*, 170–177.
94. Margulies, E.A.; Shoer, L.E.; Eaton, S.W.; Wasielewski, M.R. Excimer formation in cofacial and slip-stacked perylene-3,4:9,10-bis(dicarboximide) dimers on a redox-inactive triptycene scaffold. *Phys. Chem. Chem. Phys.* **2014**, *16*, 23735–23742.
95. Schubert, A.; Settels, V.; Liu, W.; Würthner, F.; Meier, C.; Fink, R.F.; Schindlbeck, S.; Lochbrunner, S.; Engels, B.; Engel, V. Ultrafast exciton self-trapping upon geometry deformation in perylene-based molecular aggregates. *J. Phys. Chem. Lett.* **2013**, *4*, 792–796.
96. Marciniak, H.; Li, X.Q.; Würthner, F.; Lochbrunner, S. One-dimensional exciton diffusion in perylene bisimide aggregates. *J. Phys. Chem. A* **2011**, *115*, 648–654.
97. Guo, X.; Bu, L.; Zhao, Y.; Xie, Z.; Geng, Y.; Wang, L. Controlled phase separation for efficient energy conversion in dye/polymer blend bulk heterojunction photovoltaic cells. *Thin Solid Films* **2009**, *517*, 4654–4657.
98. Li, J.; Dierschke, F.; Wu, J.; Grimsdale, A.C.; Müllen, K. Poly(2,7-carbazole) and perylene tetracarboxydiimide: A promising donor/acceptor pair for polymer solar cells. *J. Mater. Chem.* **2006**, *16*, 96–100.
99. Hartnett, P.E.; Timalina, A.; Matte, H.S.S.R.; Zhou, N.; Guo, X.; Marks, T.J. Slip-stacked perylenediimides as an alternative strategy for high efficiency nonfullerene acceptors in organic photovoltaics. *J. Am. Chem. Soc.* **2014**, *136*, 16345–16356.
100. Rajaram, S.; Shivanna, R.; Kandappa, S.K.; Narayan, K.S. Nonplanar perylene diimides as potential alternatives to fullerenes in organic solar cells. *J. Phys. Chem. Lett.* **2012**, *3*, 2405–2408.
101. Shivanna, R.; Shoaee, S.; Dimitrov, S.; Kandappa, S.K.; Rajaram, S.; Durrant, J.R.; Narayan, K.S. Charge generation and transport in efficient organic bulk heterojunction solar cells with a perylene acceptor. *Energy Environ. Sci.* **2014**, *7*, 435–441.
102. Jiang, W.; Ye, L.; Li, X.; Xiao, C.; Tan, F.; Zhao, W.; Hou, J.; Wang, Z. Bay-linked perylene bisimides as promising non-fullerene acceptors for organic solar cells. *Chem. Commun.* **2014**, *50*, 1024–1026.
103. Zang, Y.; Li, C.-Z.; Chueh, C.-C.; Williams, S.T.; Jiang, W.; Wang, Z.H.; Yu, J.S.; Jen, A.K.-Y. Integrated molecular, interfacial, and device engineering towards high-performance non-fullerene based organic solar cells. *Adv. Mater.* **2014**, *26*, 5708–5714.
104. Zhao, J.; Li, Y.; Lin, H.; Liu, Y.; Jiang, K.; Mu, C.; Ma, T.; Lin Lai, J.Y.; Hu, H.; Yu, D.; *et al.* High-efficiency non-fullerene organic solar cells enabled by a difluorobenzothiadiazole-based donor polymer combined with a properly matched small molecule acceptor. *Energy Environ. Sci.* **2015**, *8*, 520–525.
105. Zhong, Y.; Trinh, M.T.; Chen, R.; Wang, W.; Khlyabich, P.P.; Kumar, B.; Xu, Q.; Nam, C.; Sfeir, M.Y.; Black, C.; *et al.* Efficient organic solar cells with helical perylene diimide electron acceptors. *J. Am. Chem. Soc.* **2014**, *136*, 15215–15221.

106. Chen, L.; Peng, S.; Chen, Y. Cooperative assembly of pyrene-functionalized donor/acceptor blend for ordered nanomorphology by intermolecular noncovalent π - π interactions. *ACS Appl. Mater. Interfaces* **2014**, *6*, 8115–8123.
107. Beltrán, E.; Garzoni, M.; Feringán, B.; Vancheri, A.; Barberá, J.; Serrano, J.L.; Pavan, G.M.; Giménez, R.; Sierra, T. Self-organization of star-shaped columnar liquid crystals with a coaxial nanophase segregation revealed by a combined experimental and simulation approach. *Chem. Commun.* **2015**, *51*, 1811–1814.
108. Mativetsky, J.M.; Kastler, M.; Savage, R.C.; Gentilini, D.; Palma, M.; Pisula, W.; Müllen, K.; Samorì, P. Self-assembly of a donor–acceptor dyad across multiple length scales: Functional architectures for organic electronics. *Adv. Funct. Mater.* **2009**, *19*, 2486–2494.
109. Possamai, G.; Marcuz, S.; Mageini, M.; Menna, E.; Franco, L.; Ruzzi, M.; Ceola, S.; Corvaja, C.; Ridolfi, G.; Geri, A.; *et al.* Synthesis, photophysics, and photoresponse of fullerene-based azoaromatic dyads. *Chem. A Eur. J.* **2005**, *11*, 5765–5776.
110. Schwartz, P.O.; Biniek, L.; Zaborova, E.; Heinrich, B.; Brinkmann, M.; Leclerc, N.; Méry, S. Perylenediimide-based donor–acceptor dyads and triads: Impact of molecular architecture on self-assembling properties. *J. Am. Chem. Soc.* **2014**, *136*, 5981–5992.
111. Kim, J.B.; Allen, K.; Oh, S.J.; Lee, S.; Toney, M.F.; Kim, Y.S.; Kagan, C.R.; Nuckolls, C.; Loo, Y.L. Small-molecule thiophene-C₆₀ dyads as compatibilizers in inverted polymer solar cells. *Chem. Mater.* **2010**, *22*, 5762–5773.
112. Nierengarten, J.F. Fullerene-(π -conjugated oligomer) dyads as active photovoltaic materials. *Sol. Energy Mater. Sol. Cells* **2004**, *83*, 187–199.
113. Rajaram, S.; Armstrong, P.B.; Bumjoon, J.K.; Fréchet, J.M.J. Effect of addition of a diblock copolymer on blend morphology and performance of poly(3-hexylthiophene):perylene diimide solar cells. *Chem. Mater.* **2009**, *21*, 1775–1777.
114. Sivula, K.; Ball, Z.T.; Watanabe, N.; Fréchet, J.M.J. Amphiphilic diblock copolymer compatibilizers and their effect on the morphology and performance of polythiophene: Fullerene solar cells. *Adv. Mater.* **2006**, *18*, 206–210.
115. Kamkar, D.A.; Wang, M.; Wudl, F.; Nguyen, T.-Q. Single nanowire OPV properties of a photoconductive AFM. *ACS Nano* **2012**, *6*, 1149–1157.
116. Lee, J.U.; Jung, J.W.; Emrick, T.; Russell, T.P.; Jo, W.H. Synthesis of C₆₀-end capped P3HT and its application for high performance of P3HT/PCBM bulk heterojunction solar cells. *J. Mater. Chem.* **2010**, *20*, 3287–3294.
117. Zhang, Q.; Cirpan, A.; Russell, T.P.; Emrick, T. Donor–acceptor poly(thiophene-block-perylene diimide) copolymers: Synthesis and solar cell fabrication. *Macromolecules* **2009**, *42*, 1079–1082.
118. Miyanishi, S.; Zhang, Y.; Tajima, K.; Hashimoto, K. Fullerene attached all-semiconducting diblock copolymers for stable single-component polymer solar cells. *Chem. Commun.* **2010**, *46*, 6723–6725.
119. Leibler, L. Theory of microphase separation in block copolymers. *Macromolecules* **1980**, *13*, 1602–1617.
120. Topham, P.D.; Parnell, A.J.; Hiorns, R.C. Block copolymer strategies for solar cell technology. *J. Polym. Sci. B* **2011**, *49*, 1131–1156.

121. Matsen, M.W.; Bates, F.S. Unifying weak- and strong-segregation block copolymer theories. *Macromolecules* **1996**, *29*, 1091–1098.
122. Verduzco, R.; Botiz, I.; Pickel, D.L.; Kilbey, S.M.; Hong, K.; Dimasi, E.; Darling, S.B. Polythiophene-block-polyfluorene and polythiophene-blockpoly(fluorene-co-benzothiadiazole): Insights into the self-assembly of all-conjugated block copolymers. *Macromolecules* **2011**, *44*, 530–539.
123. Sommer, M.; Komber, H.; Huettner, S.; Mulherin, R.; Kohn, P.; Greenham, N.C.; Huck, W.T.S. Synthesis, purification, and characterization of well-defined all-conjugated diblock copolymers PF8TBT-*b*-P3HT. *Macromolecules* **2012**, *45*, 4142–4151.
124. Sommer, M.; Huettner, S.; Thelakkat, M. Donor–acceptor block copolymers for photovoltaic applications. *J. Mater. Chem.* **2010**, *20*, 10788–10797.
125. Guo, C.; Lin, Y.H.; Witman, M.D.; Smith, K.A.; Wang, C.; Hexemer, A.; Strzalka, J.; Gomez, E.D.; Verduzco, R. Conjugated block copolymer photovoltaics with near 3% efficiency through microphase separation. *Nano Lett.* **2013**, *13*, 2957–2963.
126. Bao, Z.; Dodabalapur, A.; Lovinger, A.J. Soluble and processable regioregular poly(3-hexylthiophene) for thin film field-effect transistor applications with high mobility. *Appl. Phys. Lett.* **1996**, *69*, 4108–4110.
127. Kim, D.H.; Park, Y.D.; Jang, Y.; Yang, H.; Kim, Y.H.; Han, J.I.; Moon, D.G.; Park, S.; Chang, T.; Chang, C.; *et al.* Enhancement of field-effect mobility due to surface-mediated molecular ordering in regioregular polythiophene thin film transistors. *Adv. Funct. Mater.* **2005**, *15*, 77–82.
128. Yang, H.; Shin, T.J.; Yang, L.; Cho, K.; Ryu, C.Y.; Bao, Z. Effect of mesoscale crystalline structure on the field-effect mobility of regioregular poly(3-hexyl thiophene) in thin-film transistors. *Adv. Funct. Mater.* **2005**, *15*, 671–676.
129. Woo, C.H.; Thompson, B.C.; Kim, B.J.; Toney, M.F.; Fréchet, J.M.J. The influence of poly(3-hexylthiophene) regioregularity on fullerene-composite solar cell performance. *J. Am. Chem. Soc.* **2008**, *130*, 16324–16329.
130. Nam, S.; Shin, M.; Park, S.; Lee, S.; Kim, H.; Kim, Y. All-polymer solar cells with bulk heterojunction nanolayers of chemically doped electron-donating and electron-accepting polymers. *Phys. Chem. Chem. Phys.* **2012**, *14*, 15046–15053.
131. Johnson, K.; Huang, Y.-S.; Huettner, S.; Sommer, M.; Brinkmann, M.; Mulherin, R.; Niedzialek, D.; Beljonne, D.; Clark, J.; Huck, W.T.S.; *et al.* Control of intrachain charge transfer in model systems for block copolymer photovoltaic materials. *J. Am. Chem. Soc.* **2013**, *135*, 5074–5083.
132. Ruiz-Carretero, A.; Aytun, T.; Bruns, C.J.; Newcomb, C.J.; Tsai, W.-W.; Stupp, S.I. Stepwise self-assembly to improve solar cell morphology. *J. Mater. Chem. A* **2013**, *1*, 11674–11681.
133. Aytun, T.; Barreda, L.; Ruiz-Carretero, A.; Lehrman, J.A.; Stupp, S.I. Improving solar cell efficiency through hydrogen bonding: A method for tuning active layer morphology. *Chem. Mater.* **2015**, *27*, 1201–1209.
134. Noriega, R.; Rivnay, J.; Vandewal, K.; Koch, F.P.V.; Stingelin, N.; Smith, P.; Toney, M.F.; Salleo, A. A general relationship between disorder, aggregation and charge transport in conjugated polymers. *Nat. Mater.* **2013**, *12*, 1038–1044.
135. Jørgensen, M.; Norrman, K.; Krebs, F.C. Stability/degradation of polymer solar cells. *Sol. Energy Mater. Sol. Cells* **2008**, *92*, 686–714.

136. Petersen, M.H.; Hagemann, O.; Nielsen, K.T.; Jørgensen, M.; Krebs, F.C. Low band gap poly-thienopyrazines for solar cells-Introducing the 11-thia-9,13-diaza-cyclopenta[*b*]triphenylenes. *Sol. Energy Mater. Sol. Cells* **2007**, *91*, 996–1009.
137. Krebs, F.C.; Spanggaard, H.; Kjær, T.; Biancardo, M.; Alstrup, J. Large area plastic solar cell modules. *Mater. Sci. Eng. B* **2007**, *138*, 106–111.
138. Lin, Y.; Lim, J.A.; Wei, Q.; Stefan, C.B.; Briseno, A.L.; Watkins, J.J.; Mannsfeld, S.C.B.; Briseno, A.L.; Watkins, J.J. Cooperative assembly of hydrogen-bonded diblock copolythiophene/fullerene blends for photovoltaic devices with well-defined morphologies and enhanced stability. *Chem. Mater.* **2012**, *24*, 622–632.
139. Li, F.; Yager, K.G.; Dawson, N.M.; Yang, J.; Malloy, K.J.; Qin, Y. Complementary hydrogen bonding and block copolymer self-assembly in cooperation toward stable solar cells with tunable morphologies. *Macromolecules* **2013**, *46*, 9021–9031.
140. Li, F.; Yager, K.G.; Dawson, N.M.; Jiang, Y.B.; Malloy, K.J.; Qin, Y. Stable and controllable polymer/fullerene composite nanofibers through cooperative noncovalent interactions for organic photovoltaics. *Chem. Mater.* **2014**, *26*, 3747–3756.
141. Li, F.; Yager, K.G.; Dawson, N.M.; Jiang, Y.B.; Malloy, K.J.; Qin, Y. Nano-structuring polymer/fullerene composites through the interplay of conjugated polymer crystallization, block copolymer self-assembly and complementary hydrogen bonding interactions. *Polym. Chem.* **2015**, *6*, 721–731.
142. Hiszpanski, A.M.; Lee, S.S.; Wang, H.; Woll, A.R.; Nuckolls, C.; Loo, Y.L. Post-deposition processing methods to induce preferential orientation in contorted hexabenzocoronene thin films. *ACS Nano* **2013**, *7*, 294–300.
143. Cheng, C.H.; Wang, J.; Du, G.T.; Shi, S.H.; Du, Z.J.; Fan, Z.Q.; Bian, J.M.; Wang, M.S. Organic solar cells with remarkable enhanced efficiency by using a CuI buffer to control the molecular orientation and modify the anode. *Appl. Phys. Lett.* **2010**, *97*, 083305.
144. Diao, Y.; Tee, B.C.-K.; Giri, G.; Xu, J.; Kim, D.H.; Becerril, H.A.; Stoltenberg, R.M.; Lee, T.H.; Xue, G.; Mannsfeld, S.C.B.; *et al.* Solution coating of large-area organic semiconductor thin films with aligned single-crystalline domains. *Nat. Mater.* **2013**, *12*, 665–671.
145. Witte, G.; Wöll, C. Growth of aromatic molecules on solid substrates for applications in organic electronics. *J. Mater. Res.* **2004**, *19*, 1889–1916.
146. Piris, J.; Debije, M.G.; Stutzmann, N.; Laursen, B.W.; Pisula, W.; Watson, M.D.; Bjørnholm, T.; Müllen, K.; Warman, J.M. Aligned thin films of discotic hexabenzocoronenes: Anisotropy in the optical and charge transport properties. *Adv. Funct. Mater.* **2004**, *14*, 1053–1061.
147. Lee, J.U.; Jung, J.W.; Emrick, T.; Russell, T.P.; Jo, W.H. Morphology control of a polythiophene-fullerene bulk heterojunction for enhancement of the high-temperature stability of solar cell performance by a new donor–acceptor diblock copolymer. *Nanotechnology* **2010**, *21*, 105201.
148. Yang, C.; Lee, J.K.; Heeger, A.J.; Wudl, F. Well-defined donor–acceptor rod–coil diblock copolymers based on P3HT containing C₆₀: The morphology and role as a surfactant in bulk-heterojunction solar cells. *J. Mater. Chem.* **2009**, *19*, 5416–5423.

149. Jeong, S.; Kwon, Y.; Choi, B.D.; Ade, H.; Han, Y.S. Improved efficiency of bulk heterojunction poly(3-hexylthiophene):[6,6]-phenyl-C₆₁-butyric acid methyl ester photovoltaic devices using discotic liquid crystal additives. *Appl. Phys. Lett.* **2010**, *96*, 2008–2011.
150. Paci, B.; Generosi, A.; Albertini, V.R.; Spyropoulos, G.D.; Stratakis, E.; Kymakis, E. Enhancement of photo/thermal stability of organic bulk heterojunction photovoltaic devices via gold nanoparticles doping of the active layer. *Nanoscale* **2012**, *4*, 7452–7459.
151. Nalwa, K.S.; Carr, J.A.; Mahadevapuram, R.C.; Kodali, H.K.; Bose, S.; Chen, Y.; Petrich, J.W.; Ganapathysubramanian, B.; Chaudhary, S. Enhanced charge separation in organic photovoltaic films doped with ferroelectric dipoles. *Energy Environ. Sci.* **2012**, *5*, 7042–7049.
152. Wu, C.-G.; Chiang, C.-H.; Han, H.-C. Manipulating the horizontal morphology and vertical distribution of the active layer in BHJ-PSC with a multi-functional solid organic additive. *J. Mater. Chem. A* **2014**, *2*, 5295–5303.
153. Campoy-Quiles, M.; Ferenczi, T.; Agostinelli, T.; Etchegoin, P.G.; Kim, Y.; Anthopoulos, T.D.; Stavrinou, P.N.; Bradley, D.D.C.; Nelson, J. Morphology evolution via self-organization and lateral and vertical diffusion in polymer: Fullerene solar cell blends. *Nat. Mater.* **2008**, *7*, 158–164.
154. Germack, D.S.; Chan, C.K.; Hamadani, B.H.; Richter, L.J.; Fischer, D.A.; Gundlach, D.J.; Delongchamp, D.M. Substrate-dependent interface composition and charge transport in films for organic photovoltaics. *Appl. Phys. Lett.* **2009**, *94*, 233303.
155. Xu, Z.; Chen, L.M.; Yang, G.; Huang, C.H.; Hou, J.; Wu, Y.; Li, G.; Hsu, C.S.; Yang, Y. Vertical phase separation in poly(3-hexylthiophene): Fullerene derivative blends and its advantage for inverted structure solar cells. *Adv. Funct. Mater.* **2009**, *19*, 1227–1234.
156. Wang, H.; Gomez, E.D.; Kim, J.; Guan, Z.; Jaye, C.; Fischer, D.A.; Kahn, A.; Loo, Y. Device characteristics of bulk-heterojunction polymer solar cells are independent of interfacial segregation of active layers. *Chem. Mater.* **2011**, *23*, 2020–2023.
157. Tremblay, N.J.; Gorodetsky, A.A.; Cox, M.P.; Schiros, T.; Kim, B.; Steiner, R.; Bullard, Z.; Sattler, A.; So, W.Y.; Itoh, Y.; *et al.* Photovoltaic universal joints: Ball-and-socket interfaces in molecular photovoltaic cells. *Chem. Phys. Chem.* **2010**, *11*, 799–803.
158. Kang, S.J.; Kim, J.B.; Chiu, C.Y.; Ahn, S.; Schiros, T.; Lee, S.S.; Yager, K.G.; Toney, M.F.; Loo, Y.L.; Nuckolls, C. A supramolecular complex in small-molecule solar cells based on contorted aromatic molecules. *Angew. Chem. Int. Ed.* **2012**, *51*, 8594–8597.
159. Zabula, A.V.; Sevryugina, Y.V.; Spisak, S.N.; Kobryn, L.; Sygula, R.; Sygula, A.; Petrukhina, M.A. An unsolvated buckycatcher and its first dianion. *Chem. Commun.* **2014**, *50*, 2657–2659.
160. Filatov, A.S.; Ferguson, M.V.; Spisak, S.N.; Li, B.; Campana, C.F.; Petrukhina, M.A. Bowl-shaped polyarenes as concave–convex shape complementary hosts for C₆₀- and C₇₀-fullerenes. *Cryst. Growth Des.* **2014**, *14*, 756–762.
161. Sygula, A.; Yanney, M.; Henry, W.P.; Fronczek, F.R.; Zabula, A.V.; Petrukhina, M.A. Inclusion complexes and solvates of buckycatcher, a versatile molecular host with two corannulene pincers. *Cryst. Growth Des.* **2014**, *14*, 2633–2639.